JOURNAL OF GEOPHYSICAL RESEARCH: EARTH SURFACE, VOL. 118, 706–721, doi:10.1002/jgrf.20036, 2013

Field characterization of three-dimensional lee-side airflow patterns under offshore winds at a beach-dune system

Irene Delgado-Fernandez,[1] Derek W. T. Jackson,[1] J. Andrew G. Cooper,[1] Andreas C. W. Baas,[2] J. H. Meiring Beyers,[3] and Kevin Lynch[4]

Received 17 May 2012; revised 17 January 2013; accepted 24 January 2013; published 22 May 2013.

[1] Characterization of three-dimensional (3D) airflow remains elusive within a variety of environments and is particularly challenging over complex dune topography. Previous work examining airflow over and in the lee of dunes has been restricted to two-dimensional studies and has concentrated on dune shapes containing angle of repose lee sides only. However, the presence of vegetation in coastal dunes creates topographic differences and irregular shapes that interfere with flow separation at the crest and significantly modify lee-side airflow patterns and potential transport. This paper presents the first 3D field characterization of airflow patterns at the lee side of a subaerial dune. Flow information was obtained using an array of 3D ultrasonic anemometers deployed over a beach surface during seven offshore wind events. Data were used to measure cross-shore and alongshore lee-side airflow patterns using the three dimensions of the wind vector. Distances to re-attachment were similar to previous studies, but the range of transverse incident wind directions resulting in flow separation (0+/−35°) was almost twice that previously reported (0+/−20°). Airflow reversal took place with winds as slow as 1 m s^{-1}. Transverse offshore winds generated areas of opposing wind directions both within the reversed zone and beyond re-attachment, contrary to consistent deflection in only one direction found in transverse desert dunes. Patterns of flow convergence-divergence have been reported in fluvial studies. However, while convergence was associated with weak reversal in fluvial settings, it appeared to be related to strong flow reversal here and could be produced by pressure differentials at the dune crest.

Citation: Delgado-Fernandez, I., D. W. T. Jackson, J. A. G. Cooper, A. C. W. Baas, J. H. M. Beyers, and K. Lynch (2013), Field characterization of three-dimensional lee-side airflow patterns under offshore winds at a beach-dune system, *J. Geophys. Res. Earth Surf.*, *118*, 706–721, doi:10.1002/jgrf.20036.

[2] **Table of symbols**. The subscript *i* indicates *instantaneous measurement*, and its absence corresponds to 5 min average values. The subscripts *C* and *L* stand for dune "crest" and "lee side", respectively. All values are expressed in International System Units with the exception of angles expressed in degrees.

u	Cartesian component of wind vector along x axis (m s^{-1}); aligned perpendicular to the dune crest and positive offshore
v	Cartesian component of wind vector along y axis (m s^{-1}); aligned perpendicular to u and positive alongshore to the West
w	Cartesian component of wind vector along z axis (m s^{-1}); aligned perpendicular to the horizontal plane formed by u,v and positive upwards
α	horizontal flow vector angle (angle between u,v) (°)
β	vertical flow vector angle (angle between u,w) (°)
dir_h	horizontal wind direction ($dir_h = 180 - \alpha$) (°)
dir_v	"vertical" wind direction (directional data in the U-V plane) ($dir_v = 180 - \beta$) (°)
S	wind speed (m s^{-1})
h	dune height (m)
h_r	dune height measured at the re-attachment point (m)
L	horizontal length from the dune crest to the dune toe, measured parallel to the wind direction (m)
λ	Lee-slope dune angle (°)
r	distance to re-attachment from the dune crest (m)
AR	dune aspect ratio (h/L)

Additional supporting information may be found in the online version of this article.

[1]Center for Coastal and Marine Research, School of Environmental Sciences, University of Ulster, Cromore Road, Coleraine BT52 1SA, Northern Ireland, UK.
[2]Department of Geography, King's College London, Strand, London WC2R 2LS, UK.
[3]Klimaat Consulting and Innovation Inc., Guelph, Canada.
[4]Department of Geography and Archaeology, National University of Ireland, University Road, Galway, Ireland.
[5]Department of Geography, Edge Hill University, St Helens Road, Ormskirk L39 4QP, Lancashire, UK.

Corresponding author: Irene Delgado-Fernandez, Department of Geography, Edge Hill University, St Helens Road, Ormskirk L39 4QP, Lancashire, UK. (delgadoi@edgehill.ac.uk)

2169-9003/13/10.1002/jgrf.20036

1. Introduction

[3] There has been significant progress in understanding lee-side flow dynamics of fluvial and aeolian bedforms. In rivers, the role of flow separation and reversal in bed morphology [*McLean and Smith*, 1986; *Nelson and Smith*, 1989; *Nelson et al*., 1993, 1995] and modes of sediment transport [*McLean et al*., 1994; *Venditti and Bennett*, 2000; *Kostaschuk and Villard*, 1996; *Best and Kostaschuk*, 2002] have been widely investigated. The differences between the fast flow at the dune crest and the slow flow in the recirculation cell generate eddy-like coherent structures that are "injected" in the flow downstream [*Venditti and Bauer*, 2005] and are related with macro turbulence and sediment suspension in the water column [*Best et al*., 2010]. In deserts, lee-side airflow patterns play a part in controlling spacing between migrating bedforms [*Werner and Kocurek*, 1999; *Walker and Nickling*, 2002; *Kocurek et al*., 2010], maintaining dune steepness and preventing dune erosion [*Walker*, 1999, 2000], regulating the dynamics of transverse dune interdunes [*Baddock et al*., 2007], and ejecting new barchans downwind [*Hugenholtz and Barchyn*, 2012]. Stratification on the lee side of aeolian dunes is often preserved in the rock record and hence important in geological studies [*Frank and Kocurek*, 1996a]. In coastlines with low, rounded foredune morphologies, lee-side airflows play a negligible role in sediment transport dynamics [*Nordstrom et al*., 1996; *Walker et al*., 2006] and lee-side wind speeds are often under the threshold of sand movement [*Gares et al*., 1993]. In coastlines with high, sharp-crested foredunes and relatively small grain sizes, offshore winds have the potential to deliver sediment from the beach into the foredune through the process of flow separation and reversal [*Jackson et al*., 2011], which can result in significant landward sediment transport and may account for a viable portion of the total sediment budget [*Lynch et al*., 2008, 2009, 2010]. Excellent reviews of flow patterns over dunes may be found in *Walker and Nickling* [2002], *Best* [2005a], and *Livingstone et al*. [2007].

[4] Despite this wealth of knowledge, the full characterization of three-dimensional (3D) lee-side flow and its effects on sediment transport remains elusive [*Best*, 2005b; *Jackson et al*., 2011]. Most work to date has been conducted over relatively simple two-dimensional (2D) transects, with straight dunes and smooth lee-side slopes that do not influence flow separation at the crest. Straight, regular-crested dunes are relatively easier to simulate both with water in the flume [e.g., *Engel*, 1981; *Davies*, 1982; *Nelson et al*., 1993; *Bennett and Best*, 1995; *Best and Kostaschuk*, 2002] and in the wind tunnel [e.g., *Walker and Nickling*, 2003; *Dong et al*., 2007, 2009]. The majority of lee-side flow numerical modeling has also been developed for 2D scenarios both over fluvial [e.g., *McLean and Smith*, 1986; *Nelson and Smith*, 1989] and aeolian dunes [e.g., *Armalay et al*., 1983; *Le et al*., 1997; *Parsons et al*., 2004a, 2004b; *Schatz and Herrmann*, 2006; *Safarzadeh et al*., 2009; *Bechmann and Sørensen*, 2010; *Wakes et al*., 2010]. Recent studies in natural rivers [*Parsons et al*., 2005] and flumes [*Maddux et al*., 2003; *Venditti*, 2007] suggest, however, that the spatial distribution of turbulence and the flow velocity field is strongly affected by 3D river bed morphologies. In aeolian settings, computational fluid dynamic (CFD) simulations [*Beyers et al*., 2010; *Jackson et al*., 2011; *Smyth et al*., 2011, 2012] suggest complex interactions between 3D dune morphologies and airflow, but there are currently no field data on lee-side airflow three dimensionality for transverse dunes.

[5] A principal issue in aeolian settings subjected to complex 3D lee-side airflow patterns is the need for multiple observations at relatively fine spatial resolutions compared to fluvial settings. In rivers, the focus of interest is likely more concerned with the role played by 3D bed morphologies in controlling dune shapes downstream or flow characteristics in the water column *over* the dune field [*Parsons et al*., 2005], as these are linked with considerable differences in overall flow resistance [*Venditti*, 2007] and turbulence [*Maddux et al*., 2003], and hence sediment entrainment and transport downstream. In many subaerial field settings, the interest lies within the separation zone and the strength of the reversed flow over the surface, rather than in the air column above the dune field. For example, during offshore wind events over coastal dunes with lee-side airflow separation and reversal [*Jackson et al*., 2011], the entire beach surface may be within the separating bubble. It is imperative to understand in detail those airflow processes that are within the area landward of the re-attachment point. It is the strength and spatio-temporal variability of the reversed flow and its transport potential over the surface inside the separation zone that has geomorphological implications [*Lynch et al*., 2008, 2009, 2010].

[6] Most studies on lee-side airflows have only defined the separation zone and the re-attachment point in two dimensions, and/or have inferred the extent of the wake and other lee-side airflow zones indirectly. The distance to re-attachment, for example, was identified based on overall shape of velocity profiles [*Frank and Kocurek*, 1996a], variations of shear stress [*Walker*, 2000; *Walker and Nickling*, 2003], and/or changes in wind direction [*Sweet and Kocurek*, 1990; *Walker*, 1999; *Baddock et al*., 2011; *Jackson et al*., 2011]. A spatially detailed (every 5 m) and direct, quantitative visualization of lee-side airflow zones average was conducted recently in coastal dunes by *Delgado-Fernandez et al*. [2011] using a simple comparison of average downstream (u) and vertical (w) velocities (Figure 1b). However, and despite the current availability of 3D ultrasonic anemometers (UAs) [*van Boxel et al*., 2004; *Walker*, 2005], there is no field evidence of the effect of 3D dune morphologies on the spatial and temporal variability of the 3D wind vector over the lee-side surface. This is likely related to field limitations such as the need for large numbers of UAs over a wide area to ensure appropriate spatial coverage, which supports the development of alternative approaches such as CFD simulations [*Beyers et al*., 2010; *Jackson et al*., 2011; *Smyth et al*., 2011, 2012].

[7] This paper presents comprehensive results from a 10 day field experiment conducted at the lee (beach) side of a coastal foredune using an extensive grid of UAs. The objectives of this paper are to (1) provide the first 3D quantitative flow visualization of mean lee-side airflow patterns in a field setting and compare findings with previous literature, (2) examine the geomorphologic implications of flow three dimensionality and discuss potential similarities/differences between airflow patterns observed at a coastal setting versus other environments, and (3) discuss

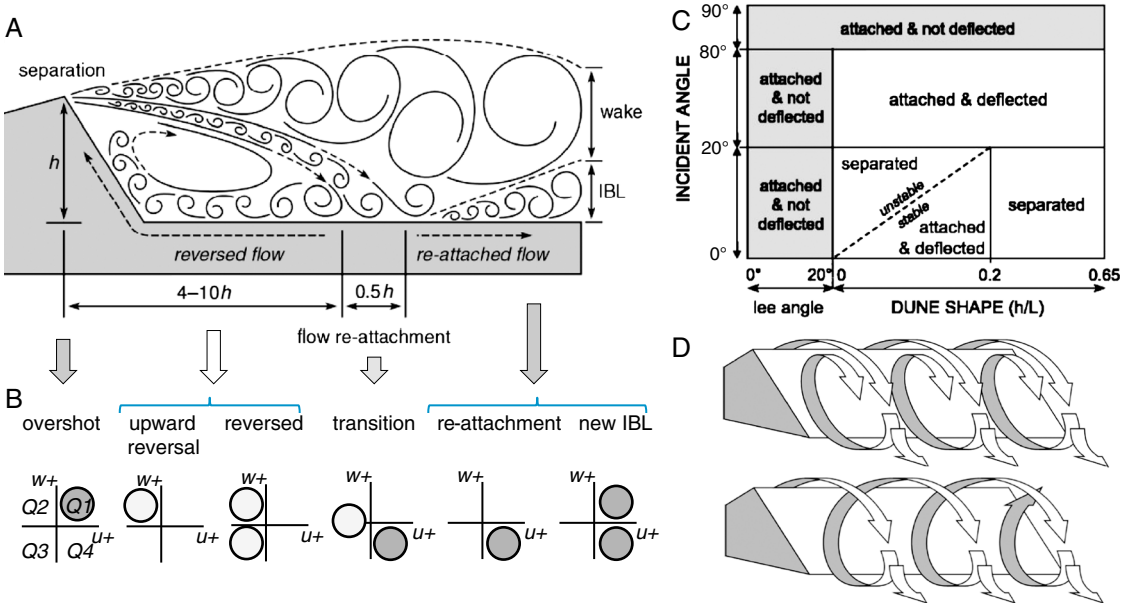

Figure 1. (A) Conceptual diagram by *Walker and Nickling* [2002] summarizing airflow patterns at the lee side of aeolian dunes; (B) Quantitative description of airflow zones at the beach surface (0.5 m) based on u, w comparisons by *Delgado-Fernandez et al.* [2011]. Gray (offshore) and white (onshore) circles highlight the quadrant (Q) favored by u, w interactions across the dune-beach transect; (C) Effect of incident wind angle (0° is normal to the dune crest), dune shape, and atmospheric stability in the type of lee-side airflows observed by *Sweet and Kocurek* [1990]; (D) Three-dimensional lee-side airflow vortices (roller - up; helical - down) described by *Allen* [1970]. Figures 1C–D correspond to modified diagrams from *Walker and Nickling* [2002], who provided condensed versions of the original figures (modified from *Walker and Nickling* [2002] with the permission of SAGE publications, from *Delgado-Fernandez et al.* [2011] with the permission of The Coastal Education & Research Foundation, and from *Sweet and Kocurek* [1990] with the permission of John Wiley and Sons).

methodological and theoretical limitations as a result of the findings presented here. Section 2 reviews models by *Walker and Nickling* [2002] and *Sweet and Kocurek* [1990] and previous findings on flow three dimensionality. Results include an analysis of 3D lee-side airflow patterns across a dune transect (section 5.1) and over a beach surface (section 5.2), and their relation with wind speed and direction and dune aspect ratio. Section 5.3 presents patterns of wind speed, and section 6.1 discusses their potential implications for sediment input to the dunes. The origin of three dimensionality and its implications in field experiments and data processing are discussed in sections 6.2 and 6.3

2. Background

2.1. 2D Description of Lee-Side Airflows

[8] As the airflow approaches a high, sharp-crested dune, it propels over the crest (overshoots) as a result of airflow compression and acceleration up the stoss slope [Figure 1A; *Walker and Nickling*, 2002]. This results in airflow separation from the underlying surface and the formation of a "wake" region within which the airflow is reversed. Downstream from the dune crest the airflow rejoins the surface (re-attachment point) at a distance (r) that varies slightly with the environment, with $r \approx 4$–8 times the dune height (h) for desert dunes [*Frank and Kocurek*, 1996b], $r \approx 5$–$10h$ for broad hills [*Cooke et al.*, 1993] and dunes simulated in wind tunnels [*Walker*, 2000], or $r \approx 4h$ from computer simulations [*Beyers et al.*, 2010; *Jackson et al.*, 2011] and coastal dunes [*Delgado-Fernandez et al.*, 2011]. The re-attachment *point* is in practice a re-attachment *zone* with an estimated width of $\approx 0.5h$ [*Walker*, 2000; *Walker and Nickling*, 2003]. An inner boundary layer (IBL) develops beyond re-attachment [*Walker and Nickling*, 2002], with implications for velocity profiles [*Frank and Kocurek*, 1996a].

[9] In an extensive study involving different dune morphologies at three desert dune fields, *Sweet and Kocurek* [1990] observed that the nature of lee-side airflows was controlled by (1) the incident wind angle at the dune crest (α_C), (2) dune shape, characterized by the lee-slope angle (λ) and the aspect ratio ($AR = h/L$, where L is the horizontal distance from the dune crest to the dune toe), and (3) atmospheric stability. Trade-offs between the three controls resulted in three broad types of lee-side airflow: (1) separated, (2) attached and deflected, and (3) attached and not deflected. Figure 1C shows a modified version by *Walker and Nickling* [2002] of the original diagram of *Sweet and Kocurek* [1990]. In general terms, airflow separation was related to α_C normal to the dune crest, increases in AR, and strong reductions in lee-side airflow speed (S_L less than 30% of incident wind speed, S_C). *Sweet and Kocurek* [1990] suggested that separated airflows switched toward "attached and deflected" at $\alpha_C > 20°$. This is a lower threshold compared to that proposed by *Allen* [1970], who attributed "roller" vortices to $\alpha_C < 45°$ and "helical" vortices to $\alpha_C > 45°$ (Figure 1D).

2.2. Three Dimensionality

[10] *Walker and Nickling* [2002] suggested that *Allen's* [1970] rollers and helical vortices are the 3D lateral extensions of the lee-side back-eddies shown in Figure 1A, which generate consistent patterns of airflow deflection and sediment transport within interdune corridors of transverse ridges [*Walker*, 1999, 2000]. Recent CFD and fluvial studies suggested, however, that the interaction between flow and crest irregularities or 3D morphologies produces recirculation zones that are strongly non-2D, with lateral flows and secondary recirculation zones [*Maddux et al*., 2003; *Best*, 2005b; *Jackson et al*., 2011].

[11] *Best* [2005a] highlighted the three dimensionality in river dune shapes and its effect on turbulence as one of the five areas where future research should focus. When present, three dimensionality generates both flow parallel and spanwise vorticity and complex areas of flow convergence and divergence [*Allen*, 1968]. Flume experiments by *Maddux et al*. [2003] showed that 3D dune morphologies were associated with larger friction coefficients but less turbulence compared to 2D dune morphologies. *Parsons et al*. [2005] also suggested that river beds with 3D dunes had smaller levels of large-scale turbulence, which could lead to less suspension of bed sediment and a reduction of overall sediment transport. A detailed flume study by *Venditti* [2003] revealed that dunes with convex (lobes) versus concave (saddles) plan forms introduced opposite effects in downstream turbulence. Lobes caused lateral and vertical divergence of momentum and energy which resulted in lower mean velocities but stronger wake regions with higher turbulent intensities. Saddles caused a convergence of flow in the hollow which resulted in less energy extraction from the mean flow, higher velocities, and decreases in turbulence, with small or absent wakes and separation zones. *Venditti* [2003] suggested that these patterns were complicated even further by the existence of regular versus irregular dune plan form shape patterns, with irregularly arranged lobes and saddle plan forms having similar effects on flow patterns. *Beyers et al*. [2010] and *Jackson et al*. [2011] used CFD techniques to simulate airflow over detailed 3D coastal dune topography and found alongshore heterogeneous patterns of airflow reversal and deflection at the beach surface. Even under directly offshore (transverse) winds, the airflow responded to dune heterogeneities in ways that would not be immediately obvious during 2D experiments concentrated along a dune cross section. Interestingly, plan form patterns of flow deflection observed by *Jackson et al*. [2011] in a coastal setting seemed opposite to those described by *Venditti* [2003] in the flume. While stronger wake regions were still associated with lower mean velocities, these areas showed flow convergence, not divergence as in the flume case.

[12] The data presented in this paper allow detailed exploration of the role of incident wind directions (α_C) and speeds (S_C) in generating lee-side separation flow and turbulence at a coastal dune site with 3D dune forms. The study area corresponds to a section of the coast with relatively small changes in h (from 10–12 m compared to desert dunes of 2–60 m studied by *Sweet and Kocurek* [1990] and thus allows only partial discussion of the role played by the *AR*. Atmospheric stability conditions can usually be considered neutral in mid-latitude coastal environments, as thermal buoyancy effects are negligible relative to the strong mechanical turbulence of the boundary layer flow.

3. Study Site

[13] Data were collected during a short-term field experiment at Magilligan Strand, Northern Ireland (Figure 2). The strand is oriented NW-SE and is approximately 6 km long. The beach is up to 100 m wide during low tide and displays a dissipative, planar topography due to the effect of high energy Atlantic swell waves [*Jackson et al*., 2005]. The coast is microtidal with a tidal range of approximately 1.6 m. Beach sediment consists predominantly of very well sorted quartz sand with a mean grain diameter of 0.17 mm. The foredune ranges in height from 6 to 12 m, and it is densely vegetated by *Ammophila arenaria* of approximately 0.4 m in height.

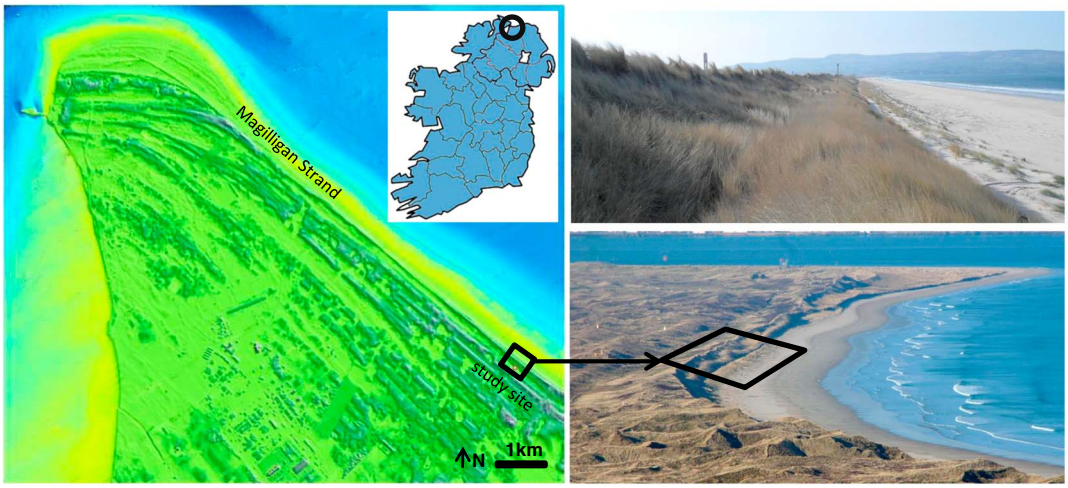

Figure 2. Location of study site at Magilligan Strand, Northern Ireland. The area of interest (square over the DEM) covered a section of approximately 100 m alongshore. The two photographs to the left show an oblique aerial view of the site (below) and the general terrain from the ground (above).

A well-formed embryo dune approximately 1 m high by 3 m wide was present at the site during the experiment. Prevailing winds are from the SW (offshore) and are thought to dominate the aeolian system [*Jackson et al*., 2011]. *Lynch et al*. [2010] reported significant secondary airflow effects at sections along Magilligan Strand where the foredune was of sufficient height (> 10 m) and the sharpness of the dune crest introduced abrupt changes in topography. Hence, the experimental site for this study was located at a section of the beach-dune system where the foredune crest reaches its highest (10–12 m) and where previous high-frequency wind measurements and CFD modelling have reported airflow separation under offshore winds [*Beyers et al*., 2010; *Jackson et al*., 2011; *Delgado-Fernandez et al*., 2011].

4. Material and Methods

4.1. Instrumentation and Data Collection

[14] The experiment was carried out between 25 April and 5 May 5, 2010. A total of seven offshore wind events were monitored, resulting in approximately 111 h of different incident wind speeds and directions. Twenty four UAs (3D Gill HS-50 model) were deployed in a grid extending 90 m alongshore by 60 m cross-shore (Figure 3). This particular field deployment was based on preliminary CFD simulations and field data indicating the extent of the reversed and re-attached zones [*Jackson et al*., 2011]. Nineteen UAs were placed at 0.5 m elevations over the beach surface (Figure 4A). The height of the UAs over the surface was similar to that adopted by *Lynch et al*. [2010] and was deemed adequate for avoiding sediment transport abrasion during strong winds while providing measurements of wind airflow close to the surface. Instruments were spaced every 10 m along profiles A, C, and D, and every 5 m along profile B. The alongshore distance between profiles was 30 m. Four UAs at elevations of 0.5, 1, 2, and 4 m over the beach surface were also deployed in a vertical array at position B2, at an approximate horizontal distance of 35 m from the dune crest (Figure 4B). This location coincided with the location of mast 6 in *Jackson et al*. [2011] where previous data suggested the presence of a well-developed area of flow reversal in the vertical. Only one vertical mast was deployed during this study to maximize the alongshore and cross-shore deployment of UAs over the beach surface. While thislimited the understanding of the vertical structure of the airflow to one location, it allowed the collection of synchronized airflow data over an extensive grid, especially near the surface where it is important for sediment transport. The most landward UA was mounted on a 6 m high mast on top of the dune crest, providing a total mean elevation of 18 m over the beach surface. Previous analysis by *Jackson et al*. [2011] suggested that wind recorded at 6 m over the dune crest was a reliable reference for free stream wind speed and direction. Some UAs located closer to the shoreline (rows 3 and 4 in Figure 3) needed to be removed during high spring tides and wave run-up which resulted in some measuring periods containing fewer UAs (Table 1). All instruments were connected through a series of terminals to a computer interface located in a trailer at the back beach at a distance far enough to avoid interference with wind measurements. Instruments measured at 25 Hz with data streamed real-time back to the central PC which allowed precise synchronization of the output files with the PC's time. A Trimble 4800 Differential Global Positioning System (DGPS) was used to map instrument positions and obtain a detailed topographic survey of the entire study site (Figure 3).

4.2. UA Data Handling

[15] UAs allow the collection of rich data sets of the three orthogonal components of the wind vector, u, v, w at very high frequencies. These may be used to derive turbulent

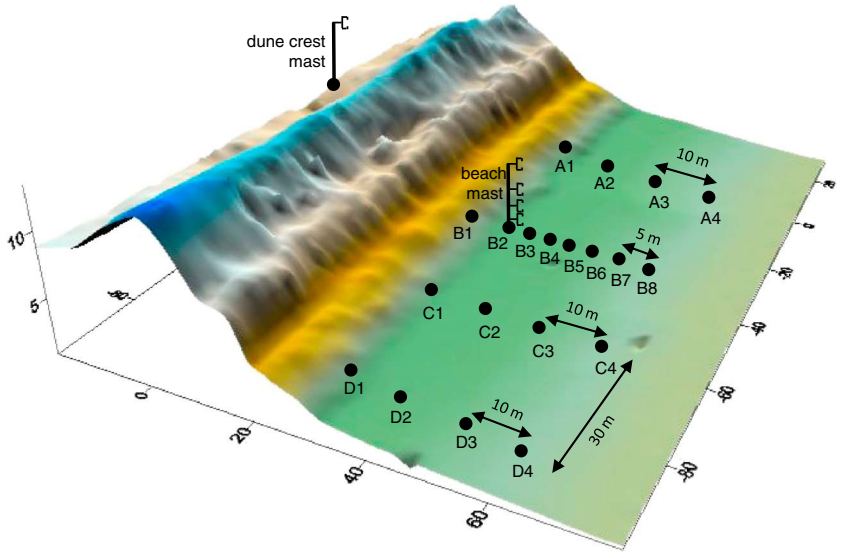

Figure 3. Topographic surface of the study site and experimental setup (vertical axis exaggerated). Black dots indicate instrument positions. The beach mast contained four ultrasonic anemometers (UAs) at elevations of 0.5, 1, 2, and 4 m over the beach surface (Figure 4B) and was located at position B2. The dune crest mast contained one UA mounted on a 6 m high mast on top of the dune crest. The horizontal distance from the dune crest mast to station B1 was approximately 30 m.

parameters such as Reynolds shear stress [*Baddock et al.*, 2011; *Weaver and Wiggs*, 2011; *Chapman et al.*, 2012] and/or to "visualize" the wind vector. While the first necessitates the rotation of the frame of reference onto the streamlines [*van Boxel et al.*, 2004; *Walker*, 2005] the second is straightforward and consists of determining the angles of the (instantaneous) wind vector relative to a "fixed" (un-rotated) coordinate system. During the experiment, UAs were oriented in the same direction at the beach and levelled with respect to the horizontal gravity plane. A right-handed Cartesian coordinate system was defined for all UAs such that u was aligned perpendicular to the dune crest and positive offshore, v was perpendicular to u and positive alongshore to the West, and w was perpendicular to the horizontal plane formed by u, v, and positive upwards. Calculation of the horizontal flow vector angle (α) (equation (1)) and the vertical flow vector angle (β) (equation (2)) were conducted over the original 25 Hz data (i.e., using instantaneous values, denoted by i). Both angles should be calculated using the *atan2* function which allows resolving angles from 0 to $\pm 180°$:

$$\alpha_i = atan2(u_i, v_i) \quad (1)$$

$$\beta_i = atan2(u_i, w_i) \quad (2)$$

[16] The instantaneous wind speed (S_i) was calculated using the three coordinates of the wind vector:

$$S_i = \left(u_i^2 + v_i^2 + w_i^2\right)^{0.5} \quad (3)$$

[17] UAs were sampled at 25 Hz, and thus the resulting time series may be used to explore high-frequency variability of any of the wind variables (u_i, v_i, w_i, S_i, α_i, β_i). For the purpose of unravelling mean streamline behavior, the original three Cartesian components of the wind vector (u_i, v_i, w_i) were averaged into 5 min records, which were subsequently used to recalculate flow angles and wind speed. Table 1 lists the number of 5 min records for each event, adding to a total of 1292 records over the seven monitored offshore wind events. The minimum wind speed at the dune crest, S_C, was 0.8 m s^{-1}, and the maximum was 15.5 m s^{-1}. Wind direction at the dune crest was variable with 80% of the winds approaching the dune at an incident angle of $\alpha_C \approx 6$ to $-90°$. Similar to the procedure adopted by *Jackson et al.* [2011], it was possible to bin 5 min records depending on α_C and isolate corresponding synchronized records at each of the sensor locations, which permits exploration of lee-side airflow patterns under different wind scenarios. These were graphed using directional data in the horizontal (dir_h) and vertical (dir_v) planes which were obtained from the opposites of the horizontal ($dir_h = 180$ - $\alpha\alpha$) and vertical ($dir_v = 180 - \beta$) wind angles, respectively. Note that while the resultant 5 min average *uvw* wind vector could be plotted alone at measurement locations, the large amount of 5 min records conveyed in the resulting figures would have made the graphs illegible. Alternatively, a mean *uvw* wind vector could have been plotted for each of the wind scenarios presented in section 5, but this would have hampered rich information on the variability of wind directionality at each of the sensors locations. Hence, and in line with a number of studies [e.g., *Sweet and Kocurek*, 1990; *Lynch et al.*, 2009, 2010; *Jackson et al.*, 2011], conventional wind roses were used to present the full degree of wind vertical and horizontal variability at each of the sensors locations (Figures 6–9). Supporting information for this article contains three tables with the values of flow vectors at each of the sensors locations.

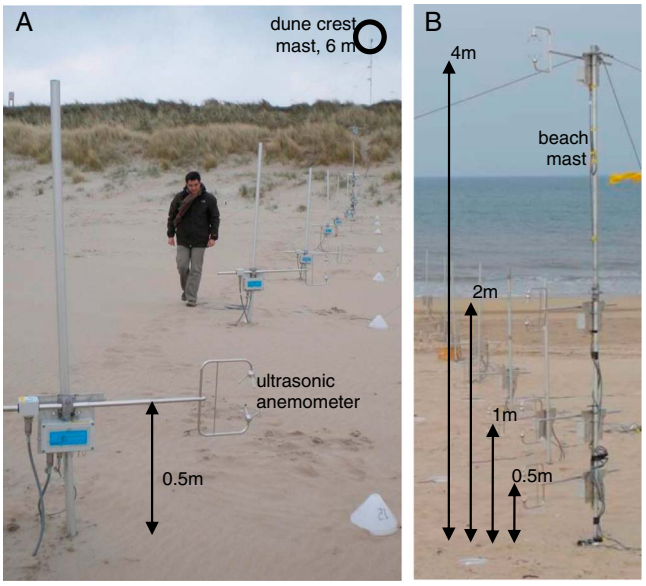

Figure 4. (A) Close-up on station B8. Ultrasonic anemometers (UAs) were deployed at 0.5 m elevation over the beach surface; (B) Close-up on beach mast at B2, containing a vertical array of UAs at different elevations over the beach surface. See Figure 3 for relative location.

Table 1. Summary of Data Collected During the Experiment in April–May 2010[a]

Event	Date - Duration	N. of UAs	N. 5 min records	α_C range	S_C range
1	25 April – 3.2h	21	37	−32 to −15	3.7–7.8
2	25 April – 20.7h	21	248	−173 to 176	1.8–7.6
3	27 April – 23.3h	17	280	−32 to 22	4.5–15.5
4	29 April – 16.2h	13	198	−105 to 145	0.9–5.9
5	3 May – 21h	24	266	−145 to −37	0.8–9.6
6	4 May – 4.2h	24	37	−91 to −57	3.5–7.6
7	4 May – 18.2h	24	226	−167 to 154	2.1–6.7

[a]The total duration of all events was ≈ 111 h (1292 5 min records); UA: 3D ultrasonic anemometer; α_C: incident horizontal wind angle (°), positive when the airflow is deflected anticlockwise (in a top-down view) from crest-normal ($\alpha_C = 0°$); S_C: wind speed (m s^{-1}) at the dune crest.

4.3. Morphological Parameters

[18] Dune morphological attributes were measured after *Sweet and Kocurek* [1990]. Figure 5 displays profiles A–D and the definition of dune height (h), length (L), and lee-side slope angle (λ) adapted for this study. An accurate quantification of these three parameters may be difficult in coastal foredunes as it involves oversimplifications and the use of relatively undefined boundaries. The majority of desert dunes monitored by *Sweet and Kocurek* [1990] presented a lee-side face with considerably long distances and gentle slopes ($< 10°$) between the dune crest and the dune brink, and steep slopes from the brink to the dune toe. Thus, those authors measured λ as the angle between the *brink-to-toe* face and the horizontal plane. Many desert and asymmetrical fluvial dunes are characterized by angle of repose lee-side slopes of 20–35° that generate well-developed separation zones of permanent, recirculating flow [*Bagnold*, 1941; *Sweet and Kocurek*, 1990; *Roden*, 1998; *Kostaschuk*, 2000, *Best and Kostaschuk*, 2002]. However, seaward faces of foredunes are often quite complex with morphologies that reflect the combined effect of processes other than wind and aeolian transport. These include wave scarping or vegetation growth, which can produce dune sections with considerably larger seaward angles. Profile B in Figure 5, for example, reflects a history of recent foredune erosion by waves, followed by the growth of an embryo dune at approximately 10 m and the subsequent growth of a newer embryo dune at approximately 25 m from the foredune crest taking place over 2 years. The location of the dune toe is also somewhat difficult to define as the dune-beach intersection may lack a sharp change in slope, especially when a dune ramp or embryo dune is present. Also, the beach itself is not usually flat, which affects the relation between the dune crest height and the distance to re-attachment (r). Due to beach slope, the dune crest elevation measured at the re-attachment point (h_r) may be considerably higher than that measured at the dune toe (h). This changes the relation $r = Xh$ (see section 2.1), X being the "number of dune heights" needed to reach the re-attachment point. As it is not possible to measure h_r prior to knowing r itself, and AR is a morphological descriptor, h was used in calculations of morphological parameters, and h_r was used in comparisons with observed r. Finally, L (and hence λ) depends on α_C, and so it was measured parallel to the incident wind direction. Dune steepness and the presence of vegetation preclude differences in the distance to re-attachment due to grain size differences [*Engel*, 1981]. Table 2 summarizes measured and calculated morphological values considered in this study.

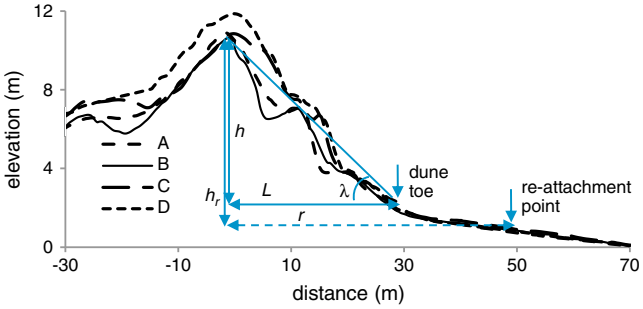

Figure 5. Topographic profiles (3 x vertical exaggeration) corresponding to transects A to D (see Figure 3) and definition of morphological parameters adapted from *Sweet and Kocurek* [1990], using profile B as an example. h: dune height; L: horizontal distance from the dune crest to the dune toe; λ: lee-side slope, angle formed between the *foredune crest-to-dune-toe* face and the horizontal plane (i.e., $\lambda = \text{atan}(h/L)$; AR: aspect ratio ($h/L$); r: distance to re-attachment; h_r: dune height measured at the re-attachment point. Note that h is a morphological descriptor, and thus it is used for the purpose of calculating AR and λ; h_r is used for relations with the distance to re-attachment.

5. Results

5.1. Quantitative 3D Airflow Visualization Across a 2D Transect

[19] Figure 6 displays results for $\alpha_C = 0+/-5°$ along profile B, where the location of UAs every 5 m allowed detailed monitoring of lee-side airflow zones. In line with previous studies [*Walker and Nickling*, 2002; *Delgado-Fernandez et al*., 2011], dir_v (cross-section view) followed a series of complex patterns that resulted in overshoot (positive β) at the dune crest and airflow re-attachment (negative β) at a distance of approximately 45 m from the dune crest ($r \approx 4.3h_r$). This fits well with observations by *Frank and Kocurek* [1996] and *Walker* [2000] in aeolian dunes, *McLean and Smith* [1986] and *Nelson and Smith* [1989] in fluvial dunes, and CFD simulations by *Jackson et al*. [2011], with re-attached zones of 4–8h. The transition from reversed airflow (40 m) to re-attached airflow (45 m) was clear both from the increase in dir_h variability (plan view) and opposite dir_v (cross section view). Vertical directions, however, showed a sharper zonation and suggested that the transition zone might be more defined and slightly narrower ($\approx 0.4h$) than that observed in previous studies [e.g., *Walker and Nickling*, 2002]. The IBL zone was characterized by a series of downward and upward streamline movements

Table 2. Numerical Values for the Morphological Variables Used in This Study[a]

Pr.	h	L_0	λ_0	AR_0	r_0	$h_{r,0}$	L_{-25}	λ_{-25}	AR_{-25}	r_{-25}	$h_{r,-25}$	L_{-50}	λ_{-50}	AR_{-50}	r_{-50}	$h_{r,-50}$
A	8.9	32	0.28	0.28	40–45	10	37	0.24	0.24	40–45	10	49	0.18	0.18	40–45	10
B	9.1	31	0.29	0.29	45	10.5	37	0.24	0.25	45	10.5	49	0.18	0.18	NA	NA
C	8.9	30	0.3	0.3	45–55	10.5	37	0.24	0.24	50–55	10.5	49	0.18	0.18	NA	NA
D	9.9	28	0.35	0.35	50–55	11.1	37	0.26	0.27	45–55	11.1	49	0.2	0.2	NA	NA

[a]See Figure 5 for definitions; h: dune height (m); L: dune length (m); λ: lee-side (seaward) slope (°); AR: aspect ratio; r: distance to re-attachment (m); h_r: dune height at the re-attachment point (m); Pr: profile number. Subscripts 0, −25, and −50 indicate corresponding incident horizontal wind angles at the dune crest (α_C). No clear flow reversal was observed in profiles B–D for $\alpha_C = -50$ (NA stands for "not applicable").

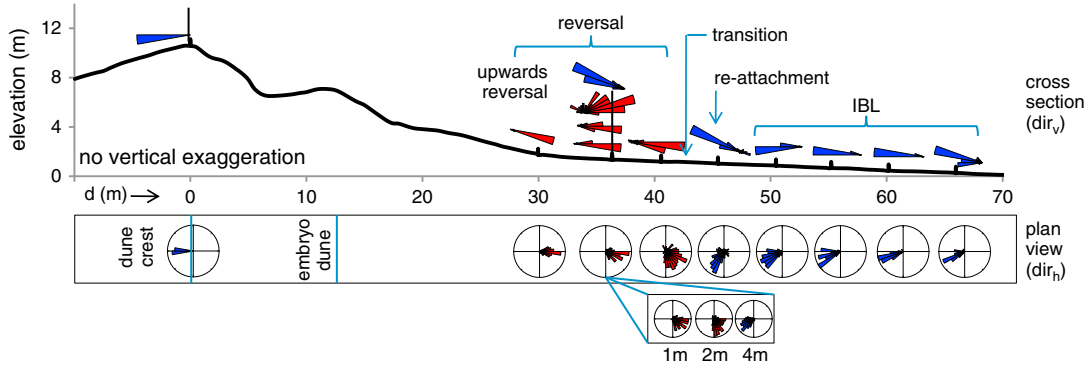

Figure 6. Quantitative description of lee-side airflow zones during perpendicular offshore winds ($\alpha_C \approx 0°$). Onshore ($-u$) directed airflow is in red; offshore ($+u$) directed airflow is in blue. Wind roses do not contain information about wind speed at each location; this is dealt with in section 5.3 and Figure 10. Sensors located at a distance (d) of 30 to 40 m showed airflow reversal, while clear re-attachment was visible at 45 m, suggesting the existence of a narrow transition zone between 40 and 45 m. A new inner boundary layer (IBL) formed beyond re-attachment with airflow at 60 and 65 m showing relative directions similar to that at the dune crest. Mean, maximum, and minimum values for flow angles at each of the sensors locations may be found in Table 4 of supporting information for this article.

(see section 6.2) and a gradual change of dir_h toward almost directly offshore at 60–65 m from the dune crest. Despite the constant α_C, airflow across this transect was consistently steered to the west (plan view). The vertical array of UAs suggests that the area of airflow reversal was at least 2 m high at 35 m from the dune crest.

5.1.1. Changes With Incident Wind Speed

[20] Wind speed at the dune crest (S_C) for $\alpha_C = 0+/-5°$ varied from 1 to almost 13 m s^{-1}. To explore the effects of increasing S_C, wind speeds were binned into three scenarios: "slow" ($S_C < 4$ m s^{-1}), "medium" ($4 \leq S_C < 8$ m s^{-1}), and "fast" ($S_C \geq 8$ m s^{-1}). Figure 7 shows wind angles along profile B for the three cases and ranges of wind speed at the dune lee side (S_L) at 30 (reversed), 45 (re-attached), and 65 m (IBL) distances from dune crest. There was no relation between increasing S_C and the location of the main lee-side airflow zones in general. UAs positioned at 30, 35, and 40 m were consistently within the reversed zone, and UAs beyond 50 m were within the re-attached zone, regardless of wind speed at the dune crest. The only sensor that reflected changes was the UA at 45 m, which recorded dir_h and dir_v characteristic of a transition zone during low S_C, but shifted to re-attachment during medium and high S_C. At low S_C, the transition zone was ≈ 10 m and contained wind speeds of $S_L = 0.5^{-1}.3$ m s^{-1}. At $S_C > 4$ m s^{-1}, the transition zone narrowed to less than 5 m and a clearer re-attachment point with faster wind speeds appeared at 45 m. The degree of dir_h steering at 40 m also varied. The wind was onshore in the three cases but more oblique at high S_C. Interestingly, S_L was very similar along the profile under the three different scenarios. Further research with wind speeds faster than the ones recorded here is needed, but the results suggest that lee-side airflow zones existed at approximately the same distance downwind from the dune crest under winds of $S_C < 4$ m s^{-1} and winds of S_C up to 13 m s^{-1}. Therefore, the extent of the reversed flow area under offshore events will likely be the same for fast *and* slow winds.

5.1.2. Changes With Wind Direction

[21] Figures 8A and 8B display dir_h and dir_v for oblique offshore winds from the SW, corresponding to $\alpha_C = -25°$ and $\alpha_C = -50°$ (+/−5°), respectively. The dataset did not contain enough wind data of $\alpha_C = 25°$ or $\alpha_C = 50°$ (from the South East), and thus these were not analyzed. The distribution of lee-side airflow zones during $\alpha_C = -25°$ (Figure 8A) did not change substantially with respect to $\alpha_C = 0°$. Airflow re-attachment still occurred at 45 m but the UA at 40 m showed highly variable dir_v characteristic of a transition zone. In contrast, the dir_h at this location was quite constant and was consistently deflected alongshore. Changes in the distribution of lee-side airflow zones were more clear for $\alpha_C = -50°$ (Figure 8B). The reversed zone disappeared almost completely from profile B, both cross-shore and vertically, with the only exception of a narrower and less clear zone of airflow reversal at 30 m. At this location, the airflow was directed downward and slightly onshore but mostly steered parallel to the dune toe. The extremely low variability of dir_h cross-shore contrasts with a significant variability of the dir_v, with a clear sequence of upward and downward movements beyond re-attachment (see section 6.2). In general, patterns in dir_h agree well with *Beyers et al.* [2010] and *Jackson et al.* [2011], who measured similar changes in lee-side airflows at the same location for winds of $\alpha_C = 0°$ (direction respect to the geographical north of $\approx 217°$) and $\alpha_C = -50°$ ($\approx 270°$).

5.2. Quantitative 3D Airflow Visualization Over a 3D Surface

[22] Figures 6 and 7 indicate that transitions from one zone to another may occur within less than 5 m and thus larger spacing between sensors of 10 m likely missed information along profiles A, C, and D (Figure 3). However, it is possible to assume a logical sequence of airflow processes similar to profile B in Figure 6 and approximate distances from the dune crest to different lee-side airflow zones depending on the information given by on-site sensors.

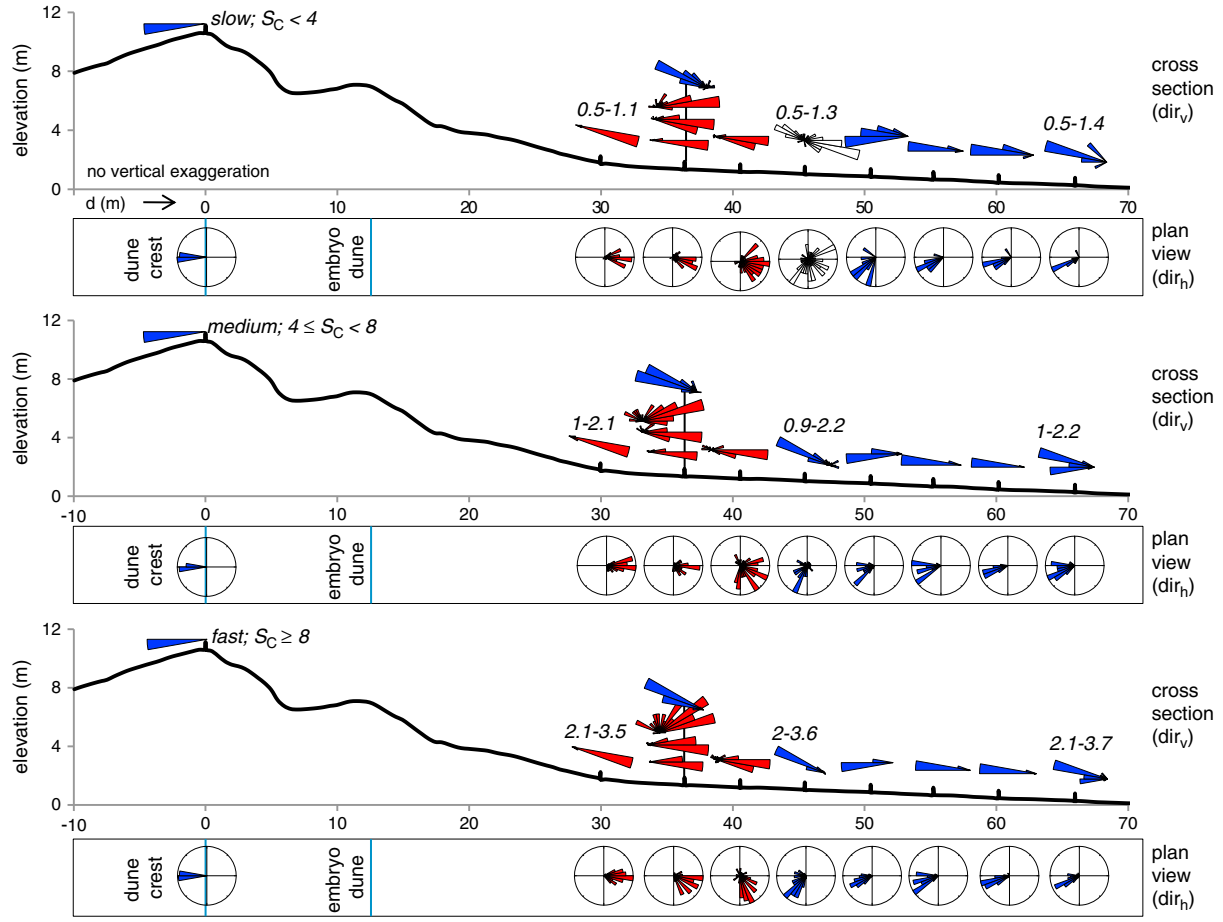

Figure 7. Airflow patterns along profile B during slow, medium, and fast wind speeds at the dune crest (S_C) for perpendicular offshore winds ($\alpha_C \approx 0°$). Onshore ($-u$) directed airflow is in red; offshore ($+u$) directed airflow is in blue. Large directional variability (characteristic of the transition zone) is represented with white roses. Values on top of particular locations indicate ranges in wind speed at the lee side (S_L). Note that the increase in S_C resulted in increases in S_L but did not modify the location of turbulent zones identified in Figure 6. All speeds are in m s^{-1}. *d*: horizontal distance.

Figure 9 shows alongshore variations of dir$_h$ and dir$_v$ for $\alpha_C = 0+/-5°$. Note that only the UAs at 35, 45, 55, and 65 m from profile B have been included in this figure as these are aligned with other sensors in the rest of the profiles. At each location, dir$_v$ (wind roses with no circular axis) have been superimposed on top of dir$_h$ (wind roses with circular axis). The sequence of lee-side airflow zones was repeated in all profiles but the distance to re-attachment (*r*) increased toward profile D. Sensors located at 45 m recorded re-attached airflow in profiles A-B, a mix of onshore-offshore directions characteristic of the transition zone in profile C, and reversed airflow in profile D. The *AR* increased slightly from profiles A to C and was largest in profile D, as a result of the increase in *h* (see Figure 5). Values of *r* were estimated by considering a range which upper limit was the position of the first sensor measuring re-attachment along a given profile and which lower limit was 5 m less (i.e. a few meters after airflow reversal or transition). The increase of *r* from profiles A (40–45 m) to D (50–55 m) seems to follow the *AR* (and hence *h*) along this section of the coastline and is in line with ranges given in other studies [e.g., *Walker and Nickling*, 2002]. Interestingly, the variability of dir$_h$ suggests complex patterns of wind steering along the beach, both within the reversed zone and beyond re-attachment. Wind directions within the reversed zone shifted from the NE in line A to the NW in line D. Similarly, dir$_h$ changed from the SE in profile A to the SW in profile D within the IBL zone. Possible explanations for this include complex submeter airflow patterns related to heterogeneities in the dune crest morphology and are discussed in section 6.2.

[23] Figures 8C and 8D display dir$_h$ and dir$_v$ for oblique offshore winds from the SW, corresponding to $\alpha_C = -25°$ and $\alpha_C = -50°$ (+/−5°) respectively. As in the cross-shore case, the distribution of lee-side airflow zones during $\alpha_C = -25°$ (Figure 8C) did not change substantially with respect to $\alpha_C = 0°$ (Figure 9). There was a clear zone of airflow reversal at the back beach and the distances to re-attachment were essentially similar. The average *AR* during $\alpha_C = -25°$ was 0.25, and there was consistent airflow steering in the same direction within the reversed zone (from the NW) and within the IBL zone (from the SW). The largest differences in dir$_v$ were registered by UAs in positions C2 and D2, which switched from transition to reversed airflow and *vice versa*. Also, similar to the cross-shore case, changes in

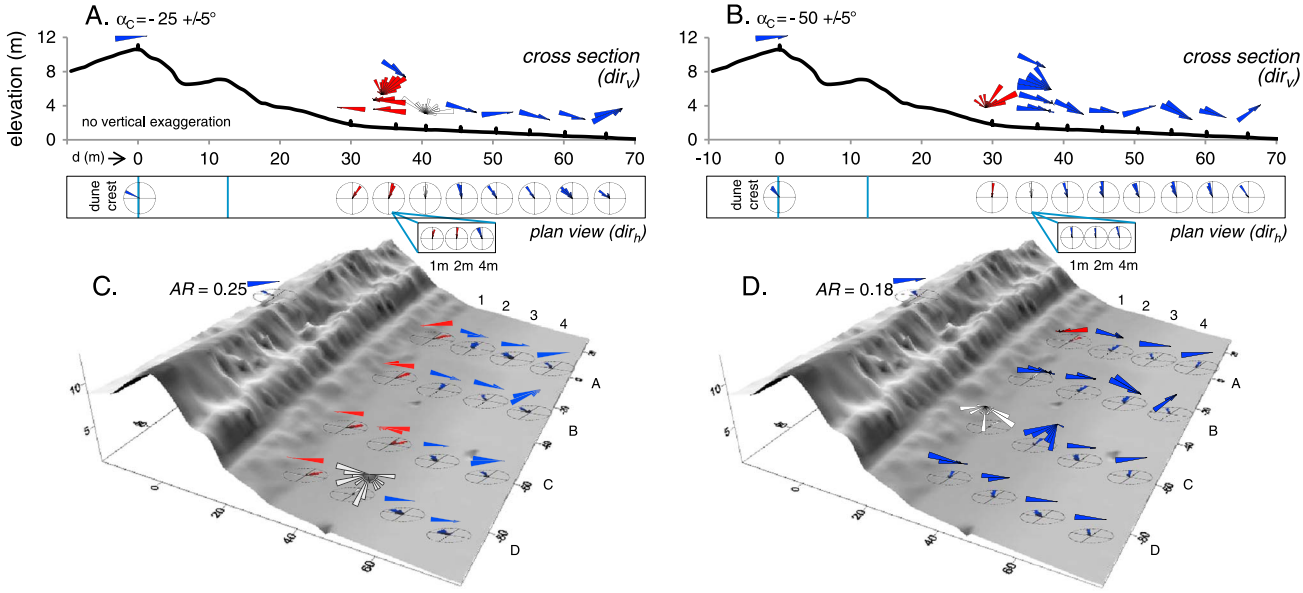

Figure 8. (A–B) Cross-shore and (C–D) alongshore variations in lee-side airflow zones associated with changes in incident wind direction at the dune crest (α_C). Circled wind roses display horizontal wind direction (dir_h); noncircled wind roses display vertical wind direction (dir_v). Onshore ($-u$) directed airflow is in red; offshore ($+u$) directed airflow is in blue. Large directional variability (characteristic of the transition zone) is represented with white roses. *AR* stands for the mean aspect ratio, and *d* is the horizontal distance across the profile. Sensors locations may be identified within the grid using the numbers on the top section of the beach and the corresponding transect letter (Figure 3). The location of lee-side airflow zones during $\alpha_C = -25 +/-5°$ was similar to that during $\alpha_C = 0 +/-5°$ (Figures 6 and 9). However, there were clear changes during $\alpha_C = -50 +/-5°$, with the reversed zone almost completely disappearing and wind directions showing less steering, suggesting deflected rather than de-attached airflows. Mean, maximum, and minimum values for flow angles at each of the sensors locations may be found in Tables 5 and 6 of supporting information for this article.

the distribution of lee-side airflow zones were clearer for $\alpha_C = -50°$ (Figure 8D), with an average $AR \approx 0.18$. The reversed zone disappeared or became quite constricted in width. The only UA that showed reversal was A1 while C1 was located within the transition zone. The change in direction at the dune crest had thus the effect of "compressing" the sequence of lee-side airflow zones (to their disappearance in some profiles) and steering the airflow parallel to the dune toe at the back beach. Finally, a strong spatial variability of upward/downward dir_v movements was clear for both scenarios, especially for $\alpha_C = -50°$. This sequence of positive and negative β angles within the IBL zone may be related to the development of complex vortex structures, which are discussed in section 6.2

5.3. Patterns of Wind Speed at the Beach Surface

[24] Previous analysis conducted by *Jackson et al.* [2011] indicated a strong relationship between S_C and S_L as measured by UAs at different locations over the beach surface, both under perpendicular and oblique offshore incident wind directions. This was confirmed by linear regression analyses conducted at all sensors locations within this study. Table 3 displays an example of some of the calculated R^2 values for $\alpha_C = 0°$, ranging from 0.73 (D3) to 0.9 (B1) with an average of 0.81 (p-values ≤ 0.0 in all cases). Results were similar for $\alpha_C = -25°$ and $\alpha_C = -50°$, with R^2 values ranging from 0.72 to 0.93. Figure 10 shows the reduction of wind speed at the beach surface with respect to that measured at the dune crest (average S_L/S_C for each UA). Wind speed at the beach was approximately 30% of that at the dune crest for $\alpha_C = 0°$ and 35% for $\alpha_C = -25°$. Wind speed patterns were more heterogeneous during $\alpha_C = -50°$, but S_L was in average approximately 50% of S_C. This is in line with results by *Sweet and Kocurek* [1990], who found that $S_L < 30\%$ under transverse winds with airflow separation.

6. Discussion

6.1. Thresholds for Changes in Lee-side Airflows and Implications for Potential Leeward Transport

[25] Analyses conducted in this paper suggest that airflow separation at the dune crest and reversal at the back beach occurred at a S_C as low as 1 to 4 m s^{-1} (Figure 7). Despite the large range of incident S_C, results did not indicate a minimum threshold of S_C at which no airflow separation occurs, which is in line with previous observations by *Sweet and Kocurek* [1990], *Walker and Nickling* [2003], and *Delgado-Fernandez et al.* [2011]

[26] Thresholds in wind direction were, however, different from values reported in the literature. *Sweet and Kocurek* [1990] suggested that $\alpha_C = 0°$ to 20° result in separated airflows for $AR > 0.2$ under neutral atmospheric conditions, and $\alpha_C = 20°$ to 80° result in attached airflow independently of the dune shape (Figure 1C). *Allen* [1970] suggested the

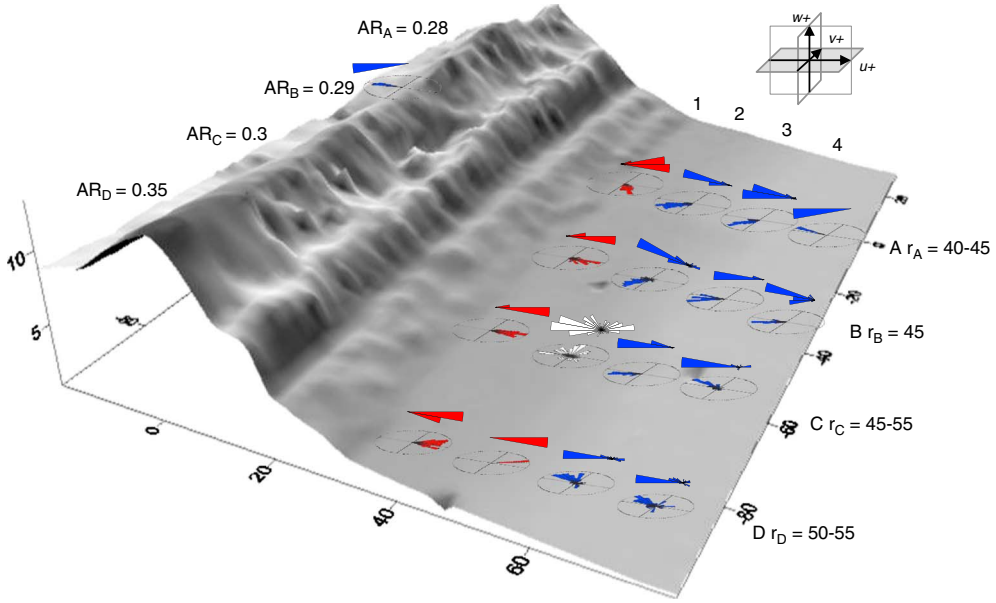

Figure 9. Alongshore variations in lee-side airflow zones during perpendicular offshore winds ($\alpha_C \approx 0°$). Circled wind roses display horizontal wind direction (dir_h); noncircled wind roses display vertical wind direction (dir_v). Onshore ($-u$) directed airflow is in red; offshore ($+u$) directed airflow is in blue. Large directional variability (characteristic of the transition zone) is represented with white roses. Sensors locations may be identified within the grid using the numbers on the top section of the beach and the corresponding transect letter (Figure 3). Both the distance to re-attachment (r) and the aspect ratio (AR) increased from profile A to D. Mean, maximum, and minimum values for flow angles at each of the sensors locations may be found in Table 4 of supporting information for this article.

Table 3. Relation Between Wind Speed at the Dune Crest and Over the Beach Surface[a]

Location	A1	A2	A3	B1	$B2_{0.5}$	$B2_1$	$B2_2$	$B2_4$	B3	B4	B5	C1	C2	C3	D1	D3
$\alpha_C = 0°$	0.81	0.83	0.83	0.9	0.85	0.83	0.85	0.83	0.83	0.8	0.75	0.81	0.83	0.77	0.77	0.73

[a]Example of R^2 values (p-values ≤ 0.0 in all cases) obtained from linear regression analysis between wind speed at the dune crest (S_C) and wind speed at different locations over the beach surface (S_L) for perpendicular offshore winds ($\alpha_C = 0°$) during event 3 (see Table 1). The number of 5 min records considered in the regression analysis was 72, and the range of S_C was 4.5–12.5 m s^{-1}. Note that with the exception of D3, all R^2 values were above 0.75, suggesting a strong relation between S_C and S_L at each of the sensors locations.

formation of closed loop roller vortexes with $\alpha_C = 0°$ to 45° and helical vortexes with $\alpha_C > 45°$ (Figure 1D). Figure 8 shows that there were no substantial changes in the location of lee-side airflow zones at the beach surface as α_C switched from 0 to −25°, but reversal almost completely disappeared from the back beach with $\alpha_C = -50°$. In order to refine the exact moment in dir_h associated with these changes, two sensors at 35 m in profiles B and D were selected (see Figure 3 for UAs locations). These recorded reversed airflows when $\alpha_C = 0°$ and $\alpha_C = -25°$ but switched to reattached airflows when $\alpha_C = -50°$. Figure 11 shows scatter plots of α_C versus β and α. At this point, all wind records have been included in the graphs, including those for onshore winds to enrich the discussion (i.e., $\alpha_C = -90°$ to −180°). Changes in β for both sensors were clear at approximately $\alpha_C = -30°$ to −40°, with a change from reversed onshore ($\beta > +/-90°$) to re-attached airflow ($\beta < +/-90°$). The wind remained re-attached for $\alpha_C = -40°$ to $\alpha_C \approx -100°$, when it "reversed" due to incident onshore winds. Changes in α showed the same trends but were more gradual. Interestingly, the airflow was never perfectly offshore at these two locations but remained steered alongshore during $\alpha_C \approx -35°$ to $\alpha_C \approx 120°$. The threshold of $\alpha_C \approx -30°$ to −40° separating reversed versus re-attached airflows at 35 m found in this study is hence half way between values reported by *Sweet and Kocurek* [1990] and *Allen* [1970] (note that comparisons are made based on absolute values, as the previous authors reported angles with no sign). Figure 8 suggests, however, that a clear distinction between separated versus attached airflow in the field may be difficult. Sensors at A1 and B1 recorded streamline slopes typical of separated and reversed airflows even under $\alpha_C = -50°$, suggesting complex mix of lee-side airflow patterns with possible coexistence of areas of separated airflow and areas of attached-deflected airflows.

[27] On average, $r \approx 45$ m for $\alpha_C = 0°$, which means that there was a relatively wide area (≈ 15 m from the embryo dune toe) of beach surface where bare sediment could have been entrained and transported back to the dune by reversed airflows (Figure 10). This area was less defined and much narrower in the case of $\alpha_C = -50°$ but contained stronger winds compared to the perpendicular case. Winds of $\alpha_C = -25°$ also resulted in a wide reversed zone, with

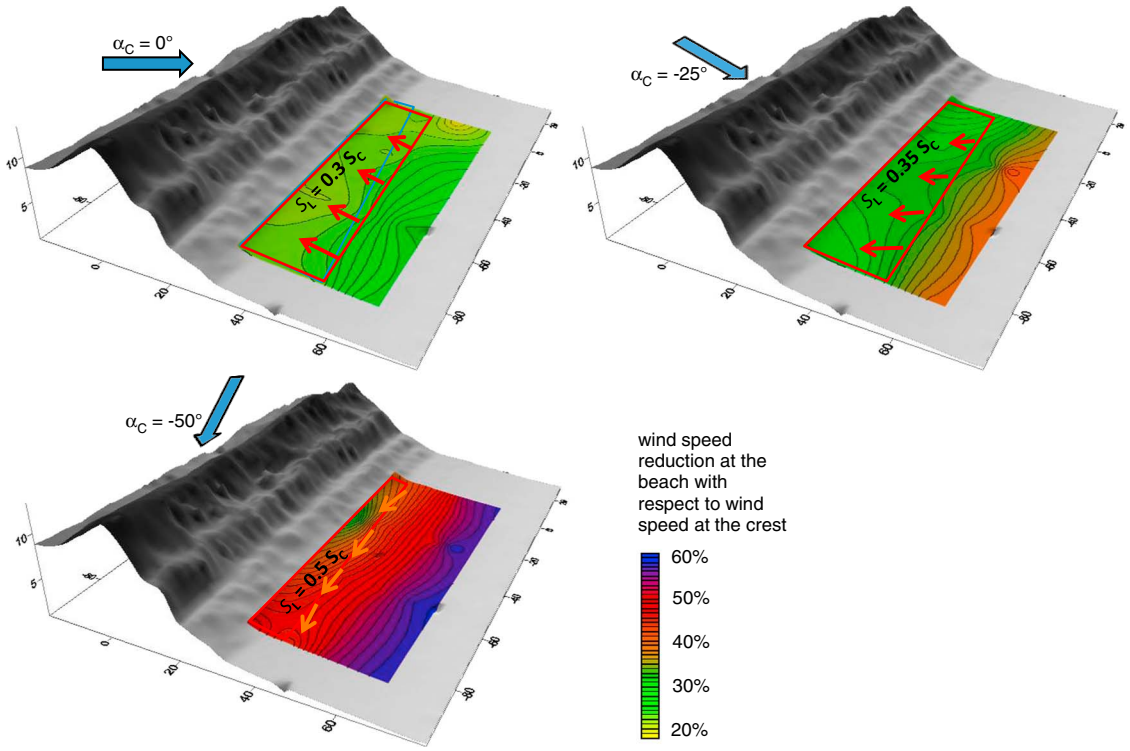

Figure 10. Wind speed reduction at the beach surface with respect to the incoming wind speed for perpendicular ($\alpha_C = 0°$), slightly oblique ($\alpha_C = -25°$), and oblique ($\alpha_C = -50°$) offshore winds. The maps show mean values of S_L/S_C at each of the sensors' locations. Contour lines are every $0.01 S_L/S_C$ (i.e., increases of 1%). S_L/S_C consistently increased away from the crest in all α_C scenarios, but the overall reduction and the range of values were different, with similar wind speeds over the beach surface (S_L) during perpendicular winds but wind speeds ranging from 30 to 60% during oblique winds. The red polygons cover an approximate area of beach surface where sediment may be transported back to the dune by reversed airflows (directionality represented by the arrows). Perpendicular offshore winds were associated with the widest area but oblique winds resulted in the strongest speeds at the back beach.

slightly faster wind speeds compared to the perpendicular case, and containing a more "steered" airflow behavior. This is there seems to be a trade-off between the size of the area containing reversed airflows and how fast they are depending on α_C. *Sweet and Kocurek* [1990] suggested that S_L could be calculated from S_C by using a cosine function of the incident α_C. This paper proposes an exponential rather the cosine function because the latest results in $S_L = 0$ m s^{-1} for $\alpha_C = 0°$. Data from sensors at 35 m used in section 6.1 (B2 and D1) were used again as an example to examine the relationship between S_L, S_C, and α_C. Figure 12 shows scatter plots of relative airflow speed (S_L/S_C) versus α_C, with the best achieved by an exponential trend line with the following general form:

$$S_L = S_C 0.26\, e^{0.01\alpha_C} \quad (4)$$

[28] *Jackson et al.* [2011] calculated the threshold shear velocity for dry sand of 0.17 mm at the site as ≈ 0.19 m s^{-1} and used this to speculate over calculations of threshold wind velocities at different heights assuming a logarithmic profile close to the surface. Details can be found in Jackson *et al.*'s section on "Geomorphological implications". Their procedure allows approximating a mean wind threshold value for dry sand at 0.5 m over the beach surface of 2.8 m s^{-1}. This corresponds to $S_C = 10.8$ m s^{-1} for $\alpha_C = 0°$, $S_C = 8.4$ m s^{-1} for $\alpha_C = -25°$, and $S_C = 6.5$ m s^{-1} for $\alpha_C = -50°$ following equation (4). Reversed airflows at Magilligan therefore have the potential to transport sediment onshore as offshore directed winds at the dune crest often exceed the calculated threshold values. This suggests that sediment budget calculations should include offshore winds at locations where dune morphology introduces airflow separation and fine sediment sizes dictate relatively lower wind thresholds for grain entrainment.

6.2. Causes of 3D Airflow Patterns

[29] Although general patterns of lee-side airflow strength and direction can be roughly depicted (previous section), results here indicate not only that the extent of the separation zone was different alongshore but also that the wind was consistently steered in opposite directions at certain locations within the similar lee-side airflow zones (section 5.3). The long distances between sensors (10 m cross-shore by 30 m alongshore) hampers a general interpretation of opposing wind directions within the reversed zone and beyond reattachment. However, it is possible to hypothesize the origin of these complex flow patterns if we assume that the field

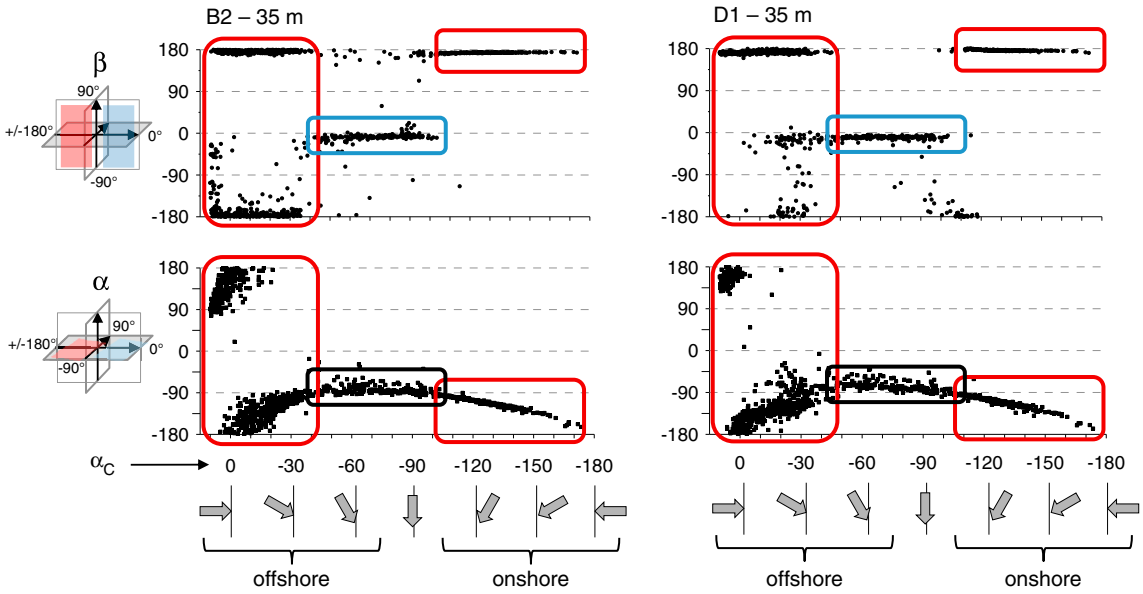

Figure 11. Scatter plots of incident horizontal wind angle at the dune crest (α_C, x axis) versus the vertical (β) and horizontal (α) angles at 35 m in profiles B and D (sensors B2 and D1 in Figure 3). A reference system has been inserted on the left side of the figure, with onshore directed airflows are in red and offshore directed airflow in blue. Black polygons isolate airflows within transition zones (oscillating between onshore and offshore). Arrows in the lower section of the figure indicate horizontal directions at the dune crest. The threshold of α_C at which both β and α showed no flow reversal was approximately at $\alpha_C \approx -30$ to $-40°$. Beyond this threshold, the airflow was attached and deflected for a range of incident α_C.

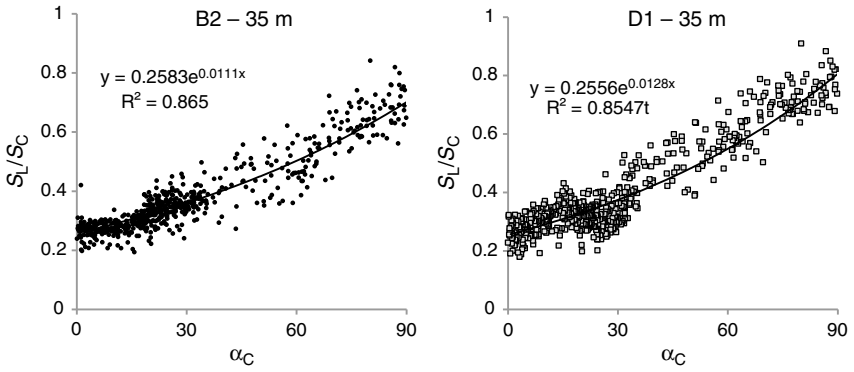

Figure 12. Scatter plots of relative flow speeds (S_L/S_C) versus incident flow angle (α_C) for sensors at 35 m in transects B and D. An exponential curve produced the best fit and suggested good correlation with R^2 values over 0.85 for both cases.

results are point measurements in the CFD map of wind velocity vector simulated by *Jackson et al.* [2011]. Figure 7 of their paper contains a 3D simulation of airflow at the same location as this field study. This map of surface velocity shows areas of flow convergence and divergence related with zones of flow reversal and no-reversal, respectively. This is opposite to the patterns associated with lobe and saddle fluvial features [*Venditti*, 2003], where flow convergence is associated with weak or absent reversal. While more research is needed, this study suggests that spatial variations of the recirculation zone may be related to both small topographic irregularities at the dune crest and with physical roughness elements introduced by the presence of vegetation. Our hypothesis suggests that relatively small protrusions on the lee-side of the dune crest that do not affect the approaching wind could have created lee-side wind pressure differentials rather than windward flow deflections. Longer recirculation lengths could therefore have been created by delayed flow separation at the crest. Shorter circulation lengths could have been caused by maintaining attached flow on the crest between protrusions. These "protrusions" are created by the presence of vegetation able to hold hummocks of sand together at slopes that would be aerodynamically unstable in bare sand. This introduces even more complexities at the lee side of coastal dunes, and could be an important factor in many deserts and rivers, where vegetation and other form of roughness elements are found.

[30] The sequences of upward/downward airflow movements (positive/negative β) within the new IBL zone may be related to the formation of complex airflow structures such as corkscrew, spiral, or hairpin vortices [*Allen*, 1985; *Ellis*, 2006]. Corkscrew vortices have been identified in many aeolian settings, from blowouts [*Hesp and Hyde*, 1996; *Smyth et al*., 2011] and desert dunes [*Greeley and Iversen*, 1985], to wind tunnel simulations [*Sutton and McKenna-Neuman*, 2008] and fluvial environments [*Best*, 2005b]. The passage of corkscrew or spiral vortices, for example, could result in alternate zones of differently pitched airflow while maintaining a fairly constant wind direction downstream (e.g., Figures 8B–C).

6.3. Logistical and Theoretical Limitations for Lee-Side Experiments

[31] As mentioned in the previous section, different beach transects showed different degrees of airflow reversal and even opposite airflow horizontal directions (e.g., compare lines a and d in Figure 9). In the absence of spatial homogeneity, 2D field experiments could provide very different results depending on the particular choice of instrument transects. This supports the need to validate powerful modelling techniques such as CFD which are able to provide a flow field over entire dune systems [*Beyers et al*., 2010; *Jackson et al*., 2011; *Smyth et al*., 2011, 2012].

[32] The processing of wind data recorded by UAs continues to be a matter of debate in the aeolian literature, with some authors choosing to calculate turbulent parameters both over rotated and nonrotated data [e.g., *Baddock et al*., 2011]. The complexity of α and β flow angles in this work supports nonrotation of lee-side airflows [in line with *Roy et al*., 1996, and *Walker*, 2005], which has consequences for the type of turbulence analyses that can be conducted in these environments. Data rotation may be applied in scenarios where it is possible to assume that the streamlines are parallel to the surface [*Roy et al*., 1996] and to each other [*Wyngaard*, 1981]. Under these conditions, it is possible to align the sensors into the streamlines, to reduce the wind spanwise (v) and vertical (w) components, and then correct the data by removing possible sensor tilts using data rotation [*Roy et al*., 1996; *Walker*, 2005]. This is important because it strongly affects the accuracy of quadrant analysis and calculated turbulent parameters such as Reynolds stress [*van Boxel et al*., 2004; *Baddock et al*., 2011; *Chapman et al*., 2012; *Lee and Baas*, 2012]. It is not possible to perform data rotation in complex situations where secondary flows induce vertical velocities different from zero because the streamlines (not the sensor) are at an angle with the surface, and where the mean vector orientation presents large spatial variability. This limits the applicability of findings in flat surfaces or at the windward slope of dunes, because the links between sediment transport and RS-quadrant analysis [*Weaver and Wiggs*, 2011] rely on the assumption that the mean vertical (normal to the bed) velocity is zero. Take, for example, the sensor located at 45 m in Figure 6, where $\alpha_C = 0+/-5°$. Previous knowledge of flow behavior at this particular location could be gathered using qualitative flow visualization techniques (e.g., smokers) or quantitative flow visualization techniques such as the one conducted in this study. According to dir_h and dir_v in Figure 6, a sensor "aligned" with the streamlines should be physically rotated roughly 50° to the right in the horizontal plane and tilted about 30° toward the beach surface. Assuming that this is possible, the calculated yaw and the pitch angles [see *van Boxel et al*., 2004; *Walker*, 2005] should be used to correct the variability between the sensor's frame of reference and the streamlines, which is roughly 70° in the *uv* plane and roughly 10° in the *uw* plane. Assuming that this is possible, the question remains as to the meaning of calculated turbulent parameters such as Reynolds stress and quadrant analysis. As *Roy et al*. point out, "what does a quadrant IV event indicate if the frame of reference adjusted to the streamline is at a 45° angle with the bed? How would these turbulent motions act with the bed sediments?" [*Roy et al*., 1996, pp. 825]. In the absence of data rotation and the presence of non-log linear velocity profiles that cannot be used to estimate friction velocity [*Sweet and Kocurek*, 1990], the lee side of aeolian dunes need new relations between transport and other turbulent parameters, such as turbulent kinetic energy, instantaneous variations in wind speed, or standard deviations of the three components of the wind vector in relation to a fixed co-ordinate system.

7. Conclusions

[33] The application of UAs in aeolian research has focused predominantly on the calculation of turbulent parameters [*van Boxel et al*., 2004; *Walker*, 2005; *Baddock et al*., 2011; Weaver *and Wiggs*, 2011; *Chapman et al*., 2012; *Lee and Baas*, 2012], the comparison of wind components in the *uv* plane [*Delgado-Fernandez et al*., 2011], and/or the calculation of wind speed and direction [*Leenders et al*., 2005; *Jackson et al*., 2011] over 2D transects. The recent work by *Smyth et al*. [2012] showing averaged measured 3D flow vectors in coastal blowouts supports the use of UAs to explore the variability of the airflow both in the *uv* (horizontal direction) and the *uw* (vertical direction) planes. This manuscript takes a step further and presents the full variability 5 min averages of wind 3D directional data at sensors' locations over an extensive grid with a spatial coverage and resolution not attempted before within the lee side of a dune. The conclusions and implications of the findings can be summarized as follow:

[34] 1. In general terms, the average distance to re-attachment ($r \approx 4h_r$) and the location of other lee-side airflow zones was relatively constant for winds approaching the dune crest at an angle of $\alpha_C = 0°$ to $-30°$ and incident wind speeds of 1 to 13 m s^{-1}. This suggests that the extent of the separation zone could remain very similar for winds blowing from a 60° window of wind directions (0+/−30°), independent of their wind speed.

[35] 2. The threshold for incident wind angle at which clear changes occurred at the beach surface was approximately at $\alpha_C = -30°$ to $-40°$, which is slightly larger than the one reported in desert dune studies. Reversed flows were stronger during oblique incident offshore winds compared to transverse offshore, winds but the size of the reversed zone was narrower. The change from transverse to oblique incident wind direction at the dune crest "compressed" the sequence of lee-side airflow zones and steered the airflow more parallel to the dune toe at the back beach.

[36] 3. The lee-side 5 min wind vector showed considerable spatial variations over the beach surface, with complex alongshore patterns of wind steering both within the reversed zone and beyond re-attachment. This suggests limited meaningfulness of data collected over 2D transects, as airflow patterns across a given profile differed substantially from those measured at another profile a few meters away alongshore, even under similar incident wind directions.

[37] 4. The location and extent of lee-side airflow zones were relatively constant under similar incident wind directions. This favors the application of CFD tools, which are capable of providing steady-state solutions of the wind field over a complex topography in three dimensions. The large number of UAs deployed in this study allowed a spatial coverage of the 3D wind vector not attempted at the lee side of a subaerial dune before. However, and despite the large grid, results highlight some of the limitations associated with measuring complex flows in the field, where sensor placement, elevation, and distance between each other limit results interpretation. CFD simulations help fill in the gaps found with point measurements and allow full sampling of coherent structures and complex airflow patterns.

[38] 5. The large variability of horizontal and vertical wind directions and the complexity of near-surface airflow vectors, with vertical flow angles of up to 30° towards the surface at the re-attachment zone, confirm the unfeasibility of performing data rotation. This precludes application of findings from windward slopes based on quadrant analysis and calculated Reynolds stress and suggests the need to investigate alternative relationships between sediment transport and turbulence at the lee side of aeolian dunes.

[39] 6. Alternative areas of airflow convergence and divergence, also visible in previous CFD simulations conducted at the same location, were associated with reversed and re-attached airflow, respectively. This is different from fluvial dunes, where flow convergence has been associated with weak or absent reversal, or from transverse desert dunes, where deflection has been reported only in one direction. Differences seem to be related to the role played by vegetation in creating topographic irregularities that are not present on bare sand dunes, and that introduce complex heterogeneities in the airflow regime.

[40] **Acknowledgments.** We wish to thank Robert Stewart, Sam Smyth, Peter Devlin, and Marianne O'Connor for their DGPS field surveying efforts. Thanks are also extended to Colin Anderson (electronics workshop), Nigel Macauley (mechanical workshop), and Thomas Smyth for providing invaluable assistance in mounting the equipment and conducting the experiment. A number of people sporadically participated and helped in the field: Ursule Boyer-Villemaire, Henk van Rein, Alexander Callaway, and Lluis Gomez-Pujol. LIDAR information was used with the permission of Geological Survey Ireland and access to the field site was kindly provided by Defence Estates UK. This work is funded through the UK Natural Environment Research Council grant NE/F019483/1.

References

Allen, J. R. L. (1968), *Current Ripples: Their Relation to Patterns of Water and Sediment Motion*, 433 pp., Elsevier, New York.

Allen, J. R. L. (1970), *Physical processes of sedimentation*, edited by J. Sutton and J. V. Watson, 248 pp., George Allen and Unwin Ltd., London.

Allen, J. R. L. (1985), *Principles of Physical Sedimentology*, 272 pp., George Allen and Unwin Ltd., London.

Armalay, B. F., F. Durst, J. C. F. Pereira, and B. Schonung (1983), Experimental and theoretical investigation of backward-facing step flow, *J. Fluid Mech.*, *127*, 473–496, doi:10.1017/S0022112083002839.

Baddock, M. C., I. Livingstone, and G. F. S. Wiggs (2007), The geomorphological significance of airflow patterns in transverse dune interdunes, *Geomorphology*, *87*, 322–326, doi.org/10.1016/j.geomorph.2006.10.006.

Baddock, M. C., G. F. S. Wiggs, and I. Livingstone (2011), A field study of mean and turbulent flow characteristics upwind, over and downwind of barchan dunes, *Earth Surf. Processes Landforms*, *36*, 1435–1448, doi:10.1002/ESP.2161.

Bagnold, R. A. (1941), *The Physics of Blown Sand and Desert Dunes*, 265 pp., Methuen, London.

Bechmann, A., and N. N. Sørensen (2010), Hybrid RANS/LES method for wind flow over complex terrain, *Wind Energy*, *13*, 36–50, doi:10.1002/we.346.

Bennett, S. J., and J. L. Best (1995), Mean flow and turbulence structure over fixed, two-dimensional dunes: implications for sediment transport and bedform stability, *Sedimentology*, *42*, 491–513, doi:10.1111/j.1365-3091.1995.tb00386.x.

Best, J. L. (2005a), The fluid dynamics of river dunes: A review and some future research directions, *J. Geophys. Res.*, *110*, F04S02, doi:10.1029/2004JF000218.

Best, J. L. (2005b), The kinematics, topology and significance of dune related macroturbulence: Some observations from the laboratory and field, in *Fluvial Sedimentology VII*, Spec. Publ. Int. Assoc. Sedimentol., 35, edited by M. D. Blum, S. B. Marriott, and S. Leclair, 7th International Conference on Fluvial Sedimentology, Lincoln, Nebraska, August 6–10, 2001, pp. 41–60, doi:10.1002/9781444304350.ch3.

Best, J. L., and R. A. Kostaschuk (2002), An experimental study of turbulent flow over a low-angle dune, *J. Geophys. Res.*, *107*, 3135, 19 pp, doi:10.1029/2000JC000294.

Best, J., S. Simmons, D. Parsons, K. Oberg, J. Czuba, and C. Malzone (2010), A new methodology for the quantitative visualization of coherent flow structures in alluvial channels using multibeam echo-sounding (MBES), *Geophys. Res. Lett.*, *37*, L06405, 6 pp, doi:10.1029/2009GL041852.

Beyers, J. H. M., D. W. T. Jackson, K. Lynch, J. A. G. Cooper, A. C. W. Baas, I. Delgado-Fernandez, and D. Pierre-Olivier (2010), Field testing and CFD LES simulation of offshore wind flows over coastal dune terrain in Northern Ireland. Fifth International Symposium on Computational Wind Engineering (CWE2010), North Carolina, US, May 23–27.

Chapman, C., I. J. Walker, P. A. Hesp, B. O. Bauer, and R. G. D. Davidson-Arnott (2012), Turbulent Reynolds stress and quadrant event activity in wind flow over a vegetated foredune, *Geomorphology*, *151*, 1–12, doi.org/10.1016/j.geomorph.2011.11.015.

Cooke, R. U., A. S. Goudie, and A. Warren (1993), *Desert geomorphology*, 526 pp., UCL Press, London.

Davies, T. (1982), Discussion of 'Length of flow separation over dunes', *J. Hydraul. Div.*, *108*, 884–885.

Delgado-Fernandez, I., D. W. T. Jackson, J. A. G. Cooper, A. C. W. Baas, K. Lynch, and J. H. M. Beyers (2011), Re-attachment zone characterisation under offshore winds blowing over complex foredune topography, *J. Coastal Res.*, SI 64, *1*, 273–277.

Dong, Z., G. Qinan, W. Luo, and H. Wang (2007), Simulation of the effects of stoss slope on the lee airflow pattern over a two-dimensional transverse dune, *J. Geophys. Res., [Earth Surf.]*, *112*, F03019, doi:10.1029/2006JF000686.

Dong, Z., G. Qinan, P. Lu, W. Luo, and H. Wang (2009), Turbulence fields in the lee of two-dimensional transverse dunes simulated in a wind tunnel, *Earth Surf. Processes Landforms*, *34*, 204–216, doi:10.1002/esp.1704.

Ellis, J. T. (2006), Coherent Structures and Aeolian Saltation, PhD Thesis, 123 pp., Dep. of Geog., Faculty Publications, Texas A&M University.

Engel, P. (1981), Length of Flow Separation over Dunes, *J. Hydraul. Div.*, *107*, 1133–1143.

Frank, A., and G. Kocurek (1996a), Toward a model of airflow on the lee side of aeolian dunes, *Sedimentology*, *43*, 451–458, doi:10.1046/J.1365-3091.1996.D01-20.X.

Frank, A., and G. Kocurek (1996b), Airflow up the stoss slope of sand dunes: Limitations of current understanding, *Geomorphology*, *17*, 47–54, doi:10.1016/0169-555X(95)00094-L.

Gares, P. A., K.-F. Nordstrom, D. J. Sherman, B. O. Bauer, R. G.-D. Davidson-Arnott, R. W. G. Carter, D. W. T. Jackson, and N. Gomes (1993), Aeolian sediment transport under offshore wind conditions: Implications for sediment budget calculations, in *Coastlines of Canada*, edited by L. P. Hildebrand, 8th Symposium on Coastal and Ocean Management, New Orleans, Lousiana, July 19–23, 1993, pp. 59–72, American Society of Civil Engineers, ISBN:10:0872629562.

Greeley, R., and J. D. Iversen (1985), *Wind as a Geological Process on Earth, Mars, Venus and Titan*, 333 pp., Cambridge University Press, London.

Hesp, P. A., and M. R. Hyde (1996), Flow dynamics and geomorphology of a trough blowout, *Sedimentology*, *43*, 505–525, doi:10.1046/j.1365-3091.1996.d01-22.x.

Hugenholtz, C. H., and T. E. Barchyn (2012), Real barchans dune collision and ejections, *Geophys. Res. Lett.*, *39*, L02306, doi:10.1029/2011GL050299.

Jackson, D. W. T., J. A. G. Cooper, and L. del Rio (2005), Geological control of beach morphodynamic state, *Mar. Geol.*, *216*, 297–314, doi.org/10.1016/j.margeo.2005.02.021.

Jackson, D. W. T., J. H. M. Beyers, K. Lynch, J. A. G. Cooper, A. C. W. Baas, and I. Delgado-Fernandez (2011), Three-dimensional wind flow behaviour over coastal dune morphology under offshore winds using Computational Fluid Dynamics (CFD) and ultrasonic anemometry, *Earth Surf. Processes Landforms*, *36*(8), 1113–1124, doi:10.1002/ESP.2139.

Kocurek, G., R. C. Ewing, and D. Mohrig (2010), How do bedform patterns arise? New views on the role of bedform interactions within a set of boundary conditions, *Earth Surf. Processes Landforms*, *35*, 51–63, doi:10.1002/esp.1913.

Kostaschuk, R. A. (2000), A field study of turbulence and sediment dynamics over subaqueous dunes with flow separation, *Sedimentology*, *47*, 519–531, doi:10.1046/j.1365-3091.2000.00303.x.

Kostaschuk, R. A., and P. Villard (1996), Flow and sediment transport over large subaqueous dunes: Fraser River, Canada, *Sedimentology*, *43*, 849–863, doi:10.1111/j.1365-3091.1996.tb01506.x.

Le, H., P. Moin, and J. Kim (1997), Direct numerical simulation of turbulent flow over a backward-facing step, *J. Fluid Mech.*, *330*, 349–374, doi:10.1017/S0022112096003941.

Lee, Z. S., and A. C. W. Baas (2012), Streamline correction for the analysis of boundary layer turbulence, *Geomorphology*, *171–172*, 69–82, doi:10.1016/j.geomorph.2012.05.005.

Leenders, J. K., J. H. van Boxel, and G. Sterk, (2005), Wind forces and related saltation transport, *Geomorphology*, *71*, 357–372, doi:10.1016/j.geomorph.2005.04.008.

Livingstone, I., G. F. S. Wiggs, and C. Weaver (2007), Geomorphology of desert sand dunes: A review of recent progress, *Earth Sci. Rev.*, *80*, 239–257, doi:10.1016/j.earscirev.2006.09.004.

Lynch, K., D. W. T. Jackson, and J. A. G. Cooper (2008), Aeolian fetch distance and secondary airflow effects: The influence of micro-scale variables on meso-scale foredune development, *Earth Surf. Processes Landforms*, *33*, 991–1005, doi:10.1002/ESP.1582.

Lynch, K., D. W. T. Jackson, and J. A. G. Cooper (2009), Foredune accretion under offshore winds, *Geomorphology*, *105*(1–2), 139–146, doi:10.1016/J.GEOMORPH.2007.12.011.

Lynch, K., D. W. T. Jackson, and J. A. G. Cooper (2010), Coastal foredune topography as a control on secondary airflow regimes under offshore winds, *Earth Surf. Processes Landforms*, *35*(3), 344–353, doi:10.1002/ESP.1925.

Maddux, T. B., J. M. Nelson, and S. R. McLean (2003), Turbulent flow over three-dimensional dunes: 1. Free surface and flow response, *J. Geophys. Res.*, *108*, 6009, doi:10.1029/2003JF000017.

McLean, S. R., and J. D. Smith (1986), A model for flow over two-dimensional bed forms, *J. Hydraul. Eng.*, *112*, 300, doi:10.1061/(ASCE)0733-9429(1986)112:4(300).

McLean, S. R., J. M. Nelson, and S. R. Wolfe (1994), Turbulence structure over two-dimensional bedforms: Implications for sediment transport, *J. Geophys. Res.*, *99*(12), 729–12,747, doi:10.1029/94JC00571.

Nelson, J. M., and J. D. Smith (1989), Mechanics of flow over ripples and dunes, *J. Geophys. Res.*, *94*, 8146–8162, doi:10.1029/JC094iC06p08146.

Nelson, J. M., S. R. McLean, and S. R. Wolfe (1993), Mean flow and turbulence fields over two-dimensional bed forms, *Water Resour. Res.*, *29*, 3935–3953, doi:10.1029/93WR01932.

Nelson, J. M., R. L. Shreve, S. R. McLean, and T. G. Drake (1995), Role of near-bed turbulence structure in bed load transport and bed form mechanics, *Water Resour. Res.*, *31*, 2071–2086.

Nordstrom, K. F., B. O. Bauer, R. G. D. Davidson-Arnott, P. A. Gares, R. W. G. Carter, D. W. T. Jackson, and D. J. Sherman (1996), Offshore aeolian transport across a beach: Carrick Finn Strand, Ireland, *J. Coastal Res.*, *12*(3), 664–672.

Parsons, D. R., G. F. S. Wiggs, I. J. Walker, R. I. Ferguson, and B. G. Garvey (2004a), Numerical modelling of airflow over an idealised transverse dune, *Environ. Modell. Softw.*, *19*, 153–162, doi:10.1016/S1364-8152(03)00117-8.

Parsons, D. R., I. J. Walker, and G. F. S. Wiggs (2004b), Numerical modelling of flow structures over idealized transverse dunes of varying geometry, *Geomorphology*, *59*, 149–164, doi:10.1016/j.gcomorph.2003.09.012.

Parsons, D. R., J. L. Best, O. Orfeo, R. J. Hardy, R. Kostaschuk, and S. N. Lane (2005), Morphology and flow fields of three-dimensional dunes, Rio Parana, Argentina: Results from simultaneous multibeam echo sounding and acoustic Doppler current profiling, *J. Geophys. Res.*, *110*, F04S03, doi:10.1029/2004JF000231.

Roden, J. E. (1998), The sedimentology and dynamics of mega-dunes, Jamuna River, Bangladesh, Ph.D. Thesis, 310 pp., Dep. of Earth Sci. and School of Geogr., Univ. of Leeds, Leeds, U. K.

Roy, A. G., P. Biron, and B. de Serres (1996), On the necessity of applying a rotation to instantaneous velocity measurements in river flows, *Earth Surf. Processes Landforms*, *21*, 817–827, doi:10.1002/(SICI)1096-9837(199609)21:9<817::AID-ESP618>3.0.CO;2–4.

Safarzadeh, A. A., S. Neyshabouri, and A. N. Dehkordi (2009), 2-D Numerical simulation of fluvial hydrodynamics and bed morphological changes, in *Computational Methods in Science and Engineering, Advances in Computational Science*, *American Institute of Physics Conference Proceedings*, 1148, edited by T. E. Simos, and G. Maroulis, *2*, pp. 739–742, doi:10.1063/1.3225424.

Schatz, V., and H. J. Herrmann (2006), Flow separation in the lee side of transverse dunes: A numerical investigation, *Geomorphology*, *81*, 207–216, doi:10.1016/j.geomorph.2006.04.009.

Smyth, T. A. G., D. W. T. Jackson, and J. A. G. Cooper (2011), Computational fluid dynamic modelling of three-dimensional airflow over dune blowouts, *J. Coastal Res.*, SI 64, *1*, 314–318.

Smyth, T. A. G., D. W. T. Jackson, and J. A. G. Cooper (2012), High resolution measured and modelled three-dimensional airflow over a coastal bowl blowout, *Geomorphology*, *177–178*, 62–73, doi:10.1016/j.geomorph.2012.07.014.

Sutton, S. L. F., and C. McKenna-Neuman (2008), Variation in bed level shear stress on surfaces sheltered by non erodible roughness elements, *J. Geophys. Res.*, *113*, F03016, doi:10.1029/2007JF000967.

Sweet, M. L., and G. Kocurek (1990), An empirical model of aeolian dune lee-face airflow, *Sedimentology*, *37*, 1023–38, doi:10.1111/j.1365-3091.1990.tb01843.x.

van Boxel, J. H., G. Sterk, and S. M. Arens (2004), Sonic anemometers in aeolian sediment transport research, *Geomorphology*, *59*, 131, doi:10.1016/J.GEOMORPH.2003.09.011.

Venditti, J. G. (2003), Initiation and development of sand dunes in river channels, Ph.D. thesis, 291 pp., Dep. of Geogr., Univ. of B. C., Vancouver, B. C., Canada.

Venditti, J. G. (2007), Turbulent flow and drag over fixed two- and three-dimensional dunes, *J. Geophys. Res.*, *112*, F04008, 21, doi:10.1029/2006JF000650.

Venditti, J. G., and B. O. Bauer (2005), Turbulent flow over a dune: Green River, Colorado, *Earth Surf. Processes Landforms*, *30*, 289–304, doi:10.1002/esp.1142.

Venditti, J. G., and S. J. Bennett (2000), Spectral analysis of turbulent flow and suspended sediment transport over dunes, *J. Geophys. Res.*, *105*, 22,035–22,047, doi:10.1029/2000JC900094.

Wakes, S. J., T. Maegli, K. J. Dickinson, and M. J. Hilton (2010), Numerical modelling of wind flow over a complex topography, *Environ. Modell. Softw.*, *25*, 237–247, doi.org/10.1016/j.envsoft.2009.08.003.

Walker, I. J. (1999), Secondary airflow and sediment transport in the lee of reversing dunes, *Earth Surf. Processes Landforms*, *24*, 437–448, doi:10.1002/(SICI)1096-9837(199905)24:5<437::AID-ESP999>3.0.CO;2-Z.

Walker, I. J. (2000), Secondary airflow and sediment transport in the lee of transverse dunes, Ph.D. Thesis, 256 pp., Dep. of Geog., Univ. of Guelph, Canada.

Walker, I. J. (2005), Physical and logistical considerations of using ultrasonic anemometers in aeolian sediment transport research, *Geomorphology*, *68*, 57–76, doi:10.1016/J.GEOMORPH.2004.09.031.

Walker, I. J., and W. G. Nickling (2002), Dynamics of secondary airflow and sediment transport over and in the lee of transverse dunes, *Prog. Phys. Geog.*, *26*, 47–75, doi:10.1191/0309133302PP325RA.

Walker, I. J., and W. G. Nickling (2003), Simulation and measurement of surface shear stress over isolated and closely spaced transverse dunes in a wind tunnel, *Earth Surf. Processes Landforms*, *28*, 1111–1124, doi:10.1016/J.GEOMORPH.2006.02.015.

Walker, I. J., P. A. Hesp, R. G. D. Davidson-Arnott, and J. Ollerhead (2006), Topographic steering of alongshore airflow over a vegetated foredune: Greenwich Dunes, Prince Edward Island, Canada, *J. Coastal Res.*, *22*(5), 1278–1291, doi:10.2112/06A.0010.I.

Weaver, C. M., and G. F. S. Wiggs (2011), Field measurements of mean and turbulent airflow over a barchan sand dune, *Geomorphology*, *128*, 32–41, doi:10.1016/J.GEOMORPH.2010.12.020.

Werner, B. T., and G. Kocurek (1999), Bedform spacing from defect dynamics, *Geology*, *27*, 727–730, doi:10.1130/0091-7613(1999)027<0727:BSFDD>2.3.CO;2.

Wyngaard, J. C. (1981), Cup, propeller, vane, and sonic anemometers in turbulence research, *Ann. Rev. Fluid Mech.*, *13*, 399–423, doi:10.1146/annurev.fl.13.010181.002151.